

New limit on an exotic parity-odd spin- and velocity-dependent interaction using an optically polarized vapor

Young Jin Kim,* Ping-Han Chu, Igor Savukov, and Shaun Newman

P-21, Los Alamos National Laboratory, P.O. Box 1663,

MS-D454, Los Alamos, NM 87545, USA

(Dated: November 4, 2022)

Abstract

Exotic spin-dependent interactions between fermions have recently attracted attention in relation to theories beyond the Standard Model of particle physics. The exotic interactions can be mediated by new fundamental spin-0 or spin-1 bosons which may explain several important unsolved mysteries in physics, such as the existence of dark matter in the Universe. In this study we expand this area of research by probing an exotic parity-odd spin- and velocity-dependent interaction between the axial-vector electron coupling and the vector nucleon coupling for polarized electrons, which has not been well explored. This experiment utilizes a highly sensitive atomic magnetometer, based on an optically polarized rubidium vapor, which is both a source of polarized electrons and a magnetic-field sensor, and a solid-state test mass containing a high density of unpolarized nucleons. By linearly moving the test mass with a constant velocity next to the rubidium vapor, an exotic interaction between the unpolarized nucleons and the polarized electrons can induce an effective magnetic field, which can be detected by the atomic magnetometer. We set an experimental limit on the electron-nucleon coupling strength of 10^{-30} at the interaction range above 10^{-3} m, corresponding to the mediator boson mass less than 10^{-4} eV. This result significantly improves the constraint for the electron-nucleon coupling strength by up to 17 orders of magnitude beyond the current limit.

* Corresponding author: youngjin@lanl.gov

The first introduction of exotic spin-dependent interactions between ordinary fermions such as electrons and nucleons dates back to 1984 [1]. To date, 15 possible exotic spin-dependant interactions have been derived by considering the spins and the relative velocity of two interacting fermions [2, 3]. In recent theoretical literature, mediators of such interactions have been generically defined as WISPs (weakly interacting sub-eV particles) [4]. The most plausible mediators are the axion and the hidden photon. The axion is a hypothetical spin-0 pseudoscalar boson that can explain the puzzling strong charge-parity (CP) problem in the quantum chromodynamics (QCD) [5–7] and is a theoretically well-motivated candidate for dark matter in the Universe [8, 9]. The hidden photon [10–12] is a spin-1 boson arising from the breaking of a new $U(1)$ gauge symmetry, which can be a dark matter candidate as well, indirectly interacting with ordinary particles [13, 14].

The detection of WISPs, including axions or hidden photons, is challenging because they are predicted to be very light in the scale of sub-eV and are only very weakly coupled to the ordinary fermions, mediating new fundamental interactions. Present axion-searching laboratory experiments such as the Axion Dark Matter eXperiment (ADMX) have been motivated by a detection approach exploiting axion-photon coupling which converts cosmic axions into photons in the presence of a strong magnetic field [15, 16]. Recently, the searches for the exotic spin-dependent interactions mediated by WISPs have attracted new attention (see the review in the Sec.VII of Ref. [17]). This type of research has been typically conducted by closely positioning two objects: one a source of ordinary fermions and the other a sensitive detector such as a superconducting quantum interference device (SQUID) [18], torsion-pendulum [19], or precessing nuclear spins in nuclear magnetic resonance (NMR) [20]. In some approaches, including the present experiments described here, the detector also serves as a source of the interacting fermions. In these cases only one local object is required, which usually enables a simpler experimental design [21, 22]. Recently, we have expanded this area of research using a highly sensitive non-cryogenic atomic magnetometer based on an optically pumped atomic vapor [22, 23]. The atomic magnetometer operates in the spin-exchange relaxation-free (SERF) regime in which the effects of spin-exchange collisions on spin relaxation are tuned off, dramatically improving the sensitivity to the femto-Tesla level [24, 25]. Our experiments probe exotic spin-dependent interactions on optically polarized electrons in an atomic vapor with unpolarized or polarized particles of a solid-state mass in the vicinity of the atomic vapor cell.

The parity-odd interaction has been discovered in the weak interaction sector [26, 27]. Searches for new parity-odd interactions, such as atomic parity non-conservation (PNC) experiments [28] and electric dipole moment (EDM) experiments [29, 30], could be pivotal for developing theories beyond the SM. In the present study we investigate an exotic parity-odd spin- and velocity-dependent interaction of electrons with axial-vector electron coupling and vector nucleon coupling ($g_A^e g_V^N$) [31], where A , V , e , and N stand for the axial-vector coupling, the vector coupling, the electron, and the nucleon, respectively. This interaction from spin-1 boson exchange can be generated by a light vector boson [32], for example, from spontaneous breaking with two or more Higgs doublets. Some experiments on the parity-odd spin- and velocity-dependent interaction of neutrons have been conducted using polarized neutrons in liquid ^4He [33], combining experimental constraints from other experiments [34] and polarized ^3He coupling to the Earth [35]. While the parity-even spin- and velocity-dependent interaction for electrons has been experimentally investigated [22, 36–39], to the best of our knowledge, the parity-odd spin- and velocity-dependent interaction of electrons has been explored by few laboratory experiments such as experiments with a torsion-pendulum [36, 37] using the Sun and the Moon as a unpolarized test mass. Our experiment applies a SERF atomic magnetometer to explore the interaction of electrons based on a similar experimental approach in Refs. [22, 23]. The experiment sets a new experimental limit on the electron-nucleon coupling strength of 10^{-30} for the vector boson mediator mass less than 10^{-4} eV, equivalent to the interaction range larger than 10^{-3} m.

RESULTS

Exotic parity-odd spin- and velocity-dependent interaction. We investigated the parity-odd spin- and velocity-dependent interaction between polarized electrons and unpolarized nucleons based on a SERF atomic magnetometer:

$$V_{12+13}(\hat{\sigma}_i, \vec{r}) = f_{12+13} \frac{\hbar}{8\pi} (\hat{\sigma}_i \cdot \vec{v}) \frac{e^{-r/\lambda}}{r}, \quad (1)$$

where \hbar is Planck's constant, $\hat{\sigma}_i$ is the i th spin unit vector of the polarized electron, $\vec{r} = r\hat{r}$ is the separation vector in the direction between the polarized electron and the unpolarized nucleon, \vec{v} is their relative velocity vector, and $\lambda = \hbar(m_a c)^{-1}$ is the interaction range (or the vector boson Compton wavelength) with m_a being the vector boson mass and c being

the speed of light in vacuum. The coupling strength constant f_{12+13} is equal to $4g_A^e g_V^N$ between electrons and nucleons for the interaction: see the definition in Ref. [31] assuming no difference between electron-neutron and electron-proton couplings, and ignoring electron-electron couplings. Equation 1 adopts the conventional numbering schemes in SI units described in Refs. [2, 31]. The interaction induces the energy shift ΔE of the polarized electrons of the alkali-metal atoms in a SERF atomic vapor, which can be recast as

$$V_{12+13} = \Delta E = \gamma \hbar \hat{\sigma}_i \cdot \vec{B}_{12+13}, \quad (2)$$

where γ is the gyromagnetic ratio of the alkali-metal atoms and \vec{B}_{12+13} is an effective magnetic field at the location of the atomic vapor, produced by the interaction V_{12+13} between the electrons and nucleons. From Eqs. 1 and 2, the effective magnetic field is

$$\vec{B}_{12+13} = f_{12+13} \frac{1}{8\pi\gamma} \vec{v} \frac{e^{-r/\lambda}}{r}. \quad (3)$$

This experiment is to detect the effective magnetic field \vec{B}_{12+13} with a SERF atomic magnetometer.

The SERF atomic magnetometer contains an atomic alkali-metal vapor cell and two laser beams (for detail, see for example the description of a SERF magnetometer in [40]). The circularly polarized “pump” laser beam serves to pump atomic spins into the stretched state, creating nearly 100% polarization. The linearly polarized “probe” laser beam serves to detect the spin projection along the probe beam. The non-zero spin projection results in the rotation of light polarization, due to the strong birefringence of the spin-polarized vapor, and is measured with a polarizing beam splitter and two photo detectors as a small difference in the balanced output. The interaction of an external magnetic field with the polarized atomic spins leads to a change in the orientations of the spins and hence in the observed light polarization rotation. Because Eq. 2 formally describes the interaction of electron spins with the effective magnetic field \vec{B}_{12+13} , the interaction V_{12+13} causes similar changes in the spin orientation as the ordinary field, and can be probed with a sensitive SERF magnetometer [22, 23].

Experimental details. We employed a commercial cm-scale SERF atomic magnetometer which is low cost, compact, and easy to operate [41, 42]. The SERF magnetometer is based on a rubidium (Rb) $3 \times 3 \times 3$ mm³ atomic vapor cell with a buffer gas. In order to operate the magnetometer in the SERF regime, the Rb vapor is heated to $\sim 160^\circ\text{C}$, which

supplies sufficiently large Rb density ($\sim 10^{13}$ Rb atoms) as the source of optically polarized electrons. Furthermore, the magnetometer was placed inside a ferrite cylindrical shield (OD=18 cm, height H=38 cm, material thickness $t=0.6$ cm) with end-caps and a three-layer open μ -metal co-axial cylinder (ID=23 cm, OD=29 cm, outer H=69 cm) as shown in Fig. 1(a). The magnetic shields sufficiently suppressed the external dc magnetic field and magnetic noise. To ensure the SERF operation regime, the residual fields inside the ferrite shield were compensated with three orthogonal coils [not shown in Fig. 1(a)]. The atomic magnetometer was rigidly mounted inside the ferrite shield by a plastic holder.

For the source of unpolarized nucleons, we used a $2 \times 2 \times 2$ cm³ non-magnetic bismuth germanate insulator (BGO), which contains a high nucleon density of 4.3×10^{24} cm⁻³. The BGO mass was provided by Rexon Components Inc. As shown in Fig. 1(a), the BGO mass was connected to a stepper motor (LR43000 manufactured by Haydon Kerk Pittman), fixed on a three-axis translation stage (Thorlabs PT3), through a 1.5 m-long rigid fiberglass G10 cylindrical rod. The motor was positioned away from the magnetic shields and was enclosed by a single-layer open μ -metal box to suppress magnetic noise arising from the motor operation [see Fig. 1(b)]. The translation stage precisely adjusted the position of the BGO mass in the vicinity of the Rb atomic vapor. In order to prevent the BGO mass from oscillating due to the movement of the long G10 rod, a non-magnetic air bushing (OAV0500IB) was closely mounted to the ferrite shield, providing an additional support of the G10 rod with nearly frictionless motion of the mass. The air pressure to the bushing was around 20 psi. To reduce systematic effects due to vibrations induced by the motor moving the BGO mass, the frame holding both the atomic magnetometer and the magnetic shields was decoupled from the frame holding the moving mass, as indicated in Fig. 1(a) and (b).

As illustrated in Fig. 1(c), the relative velocity term in the interaction V_{12+13} was created by linearly moving the BGO mass along the z -axis with a constant velocity \vec{v} next to the Rb atomic vapor located in the atomic magnetometer head. The standoff distance between the nearest surfaces of the mass and the Rb vapor cell was set to 5 mm, limited by the location of the Rb vapor cell inside the atomic magnetometer module. The Rb electron spins were oriented along the x -axis and the atomic magnetometer was sensitive to the z component of a magnetic field with the intrinsic field noise level of 15 fT/Hz^{1/2}, at low frequency. According to Eq. 3, the effective field \vec{B}_{12+13} is only along the z -axis in this configuration of the mass and the magnetometer because \vec{B}_{12+13} is proportional to \vec{v} . The Rb spins orientation is

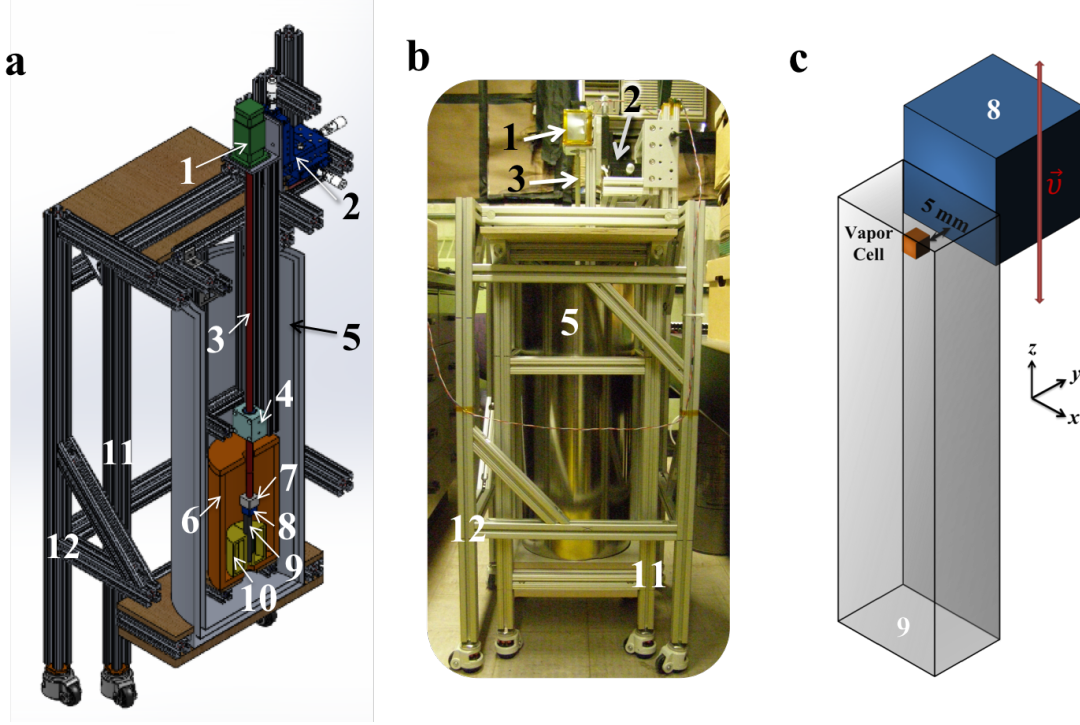


FIG. 1. The experimental setup. (a) A cutaway schematic diagram of the experimental setup to probe the interaction V_{12+13} . (b) A photograph of the experimental setup. (c) An enlarged schematic of the configuration of a unpolarized BGO mass and a SERF atomic magnetometer (scaled). In (a-c), 1 is a motor enclosed by a single-layer open μ -metal box, 2 is a three-axis translation stage, 3 is a fiberglass G10 rod, 4 is a frictionless air bushing, 5 is a three-layer open μ -metal co-axial cylindrical shield, 6 is a cylindrical ferrite shield, 7 is a sample holder, 8 is a unpolarized BGO mass, 9 is an SERF atomic magnetometer, and 10 is a plastic holder of the atomic magnetometer; 11 and 12 are aluminum frames holding the motor system moving the mass and the magnetometer/shields system, respectively. The frames are decoupled so as to reduce mechanical vibrations due to the mass motion. An unpolarized BGO mass is placed next to the Rb atomic vapor cell located inside the head of the atomic magnetometer module. The BGO mass is translated up and down in z -direction with a constant velocity \vec{v} .

changed by \vec{B}_{12+13} , which was sensitively detected by the atomic magnetometer.

Main sources of the systematic effects in this experiment are magnetic impurities buried inside the BGO mass generating fields measured on the order of 10^{-11} T and drift in the magnetometer signal on the order of 10^{-10} T. To suppress the systematic effects, the BGO mass movement was alternated to subtract the magnetometer signals between upward v and

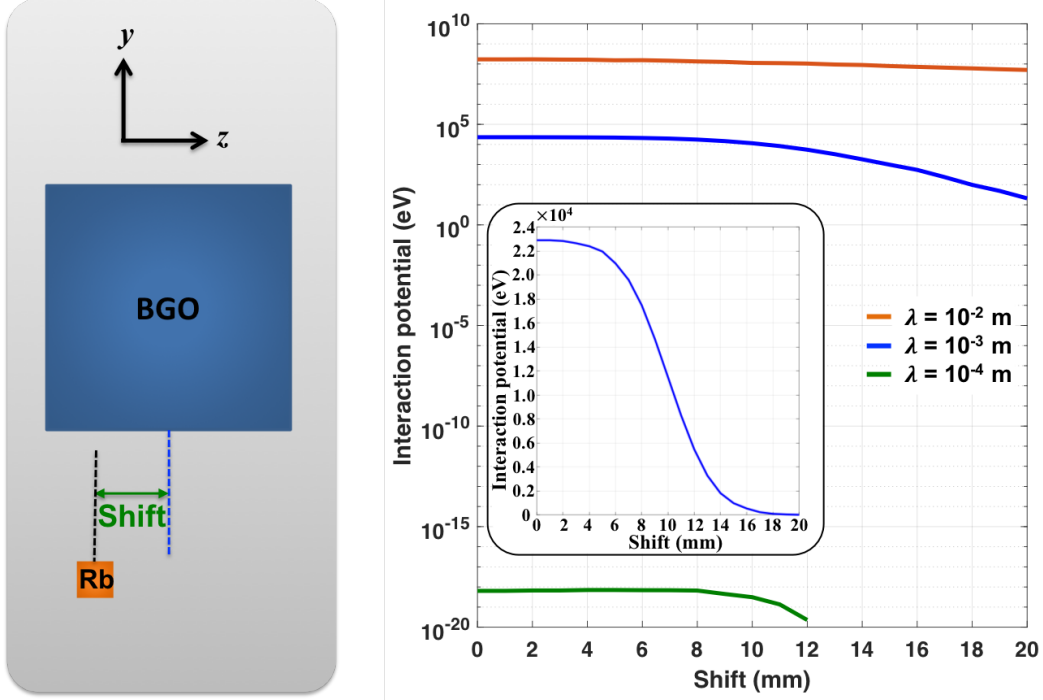


FIG. 2. The interaction potential P_{12+13} , numerically calculated by a Monte Carlo integration, as a function of the distance between the center of the BGO mass and the center of the Rb vapor cell, “Shift,” at different interaction ranges of $\lambda = 10^{-4}$, 10^{-3} , or 10^{-2} m. The vertical axis has a log scale. When the Shift = 0, the centers of the BGO mass and the Rb vapor cell are aligned. The inset enlarges the interaction potential at $\lambda = 10^{-3}$ m with the vertical axis in a linear scale. The strength of the interaction potential decreases as the BGO mass is moved away from the Rb vapor and drops more quickly at the smaller interaction range.

downward $-v$ mass motions. This technique was highly effective since the sign of \vec{B}_{12+13} is reversed for the opposite linear motions due to the single velocity term in Eq. 3, while the systematic effects are essentially the same [22].

In Fig. 2, we present the interaction potential, written as

$$P_{12+13} = \frac{\hbar}{8\pi} (\hat{\sigma} \cdot \vec{v}) \frac{e^{-r/\lambda}}{r}, \quad (4)$$

as a function of the distance between the center of the BGO mass and the center of the Rb vapor cell, defined as “Shift” here, at different interaction ranges. The interaction potential was numerically calculated by a Monte Carlo integration [22, 23] which averaged the interaction potential P_{12+13} over the both volumes of the BGO mass and the Rb vapor cell. This was done by randomly generating 2^{20} electron-nucleon pairs inside the volumes,

summing the potential P_{12+13} between each pair based on Eq. 4 by assuming the interaction range, and then normalizing the resulting potential for the nucleon density of BGO mass. More details are described below. The velocity magnitude was 15.38 mm/s, used in the present experiments. As shown in Fig. 2, the interaction potential gets weaker as the BGO mass moves away from the Rb vapor and drops more drastically for the smaller interaction range due to the term of $e^{-r/\lambda}$ in Eq. 4. Since the interaction potential varies with the position of the BGO mass with respect to the Rb vapor, we selected one proper position of the BGO mass near Shift = 0 in order to constrain the coupling constant f_{12+13} .

Analysis. In the modulation method, the BGO mass was extended along the z direction with the constant velocity of $v = 15.38$ mm/s for 0.325 s from the Shift of -1 mm to the final Shift of 4 mm, and then it was retracted toward the initial configuration with $v = -15.38$ mm/s for 0.325 s, as illustrated in Fig. 3(a). The initial configuration was chosen because the BGO sample holder contacted the head of the SERF magnetometer when Shift < -1 mm. The motor was able to repeat this BGO mass motion continuously, during which we recorded the SERF magnetometer signals for 77 hours using a 24-bit analog-to-digital converter (PXIe-4497 provided by National Instruments) with a sampling rate of 1 kHz.

The upper plot in Fig. 3(b) shows standard time traces of the SERF magnetometer signal, which present two full cycles of the BGO mass motion reversal. Here one cycle refers to one extension with $v = 15.38$ mm/s and one retraction with $v = -15.38$ mm/s of the mass. The motor provided a voltage output which allows us to distinguish the mass motion's direction, as shown in the lower plot in Fig. 3(b). This was also recorded simultaneously with the magnetometer signal. The rising and falling edges served as the reference points for each half cycle. The motor had a delay time of 0.05 s after each extension and retraction of the mass, necessary to reverse the mass motion's direction, thus the time elapsed for one cycle was 0.75 s. As discussed above, to extract the magnitude of the effective magnetic field, B_{12+13} , from the magnetometer signals, we selected the middle configuration of each motion which corresponds to Shift = 1.5 mm, as shown in Fig. 3(a), equivalent to the data point at the first 50% of the data in each half cycle, as shown in Fig. 3(b). However, instead of taking only one data point in each half cycle for the extraction of B_{12+13} , we used the mean of three data points, i.e., the data point at the first 50% of the data \pm the adjacent data points. The distance between data points is 15 μ m.

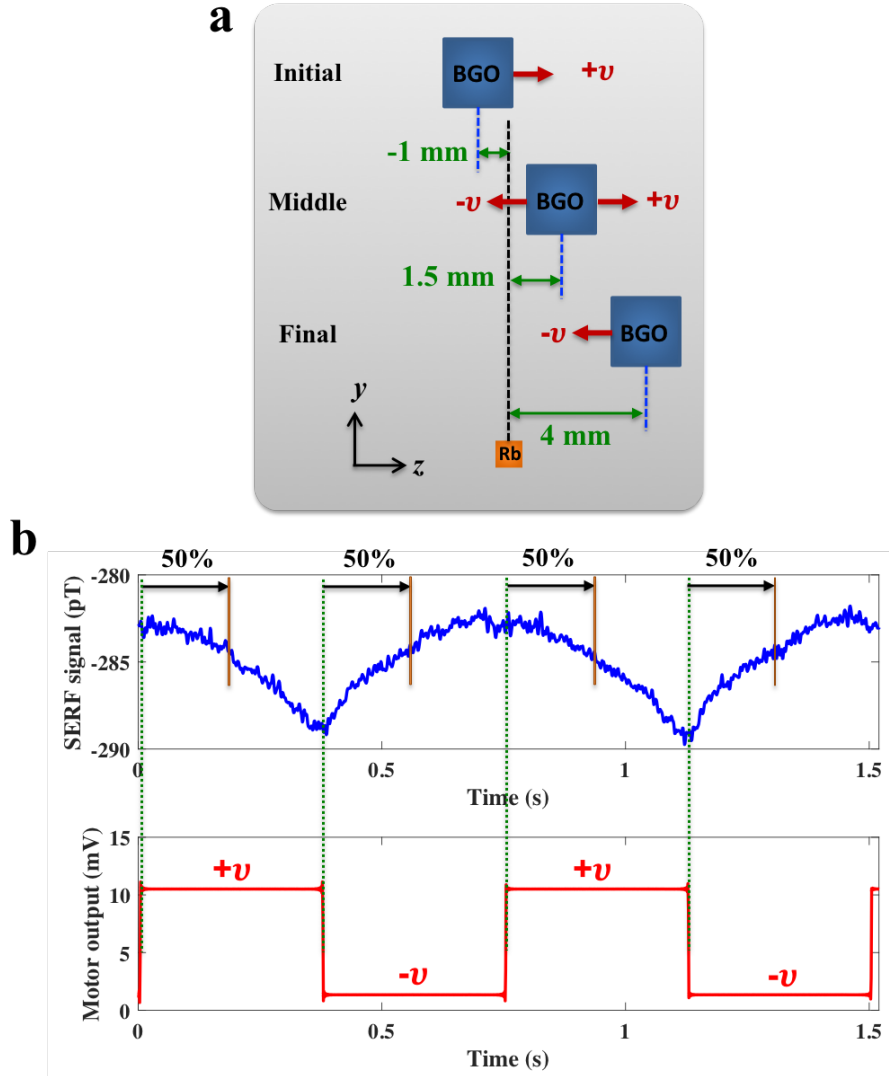


FIG. 3. Data collection. (a) A repeated BGO mass linear motion with respect to the Rb vapor (not scaled). The BGO mass was extended with $v = 15.38$ mm/s for 0.325 s and then retracted with $v = -15.38$ mm/s for 0.325 s. (b) Time traces of SERF magnetometer signal showing two full cycles of the mass linear motion reversal (upper plot) and the voltage output from the motor indicating the motion's direction (lower plot) which was high and low at extraction and retraction of the mass, respectively.

The mean value in each half cycle can be modeled as

$$D^{\pm}(t) = \pm B_{12+13} + a_0 + a_1 t + a_2 t^2 + a_3 t^3, \quad (5)$$

where the sign of $+$ and $-$ corresponds to the sign of the velocity, t is time, a_0 is the dc

offset field on the order of a few hundred pT, as shown in Fig. 3(b), and the last three terms characterize the slow drifts in the magnetometer signal expanded in a polynomial function of time up to third order. These mainly arise from magnetometer electronics and temperature variations around the magnetometer. Note that a_0 remains constant as the mass linear motion is reversed, unlike B_{12+13} . The magnetometer drift is mostly of first order: however, higher-order drifts can exist in the magnetometer signal due to, for example, opening/closing the laboratory door and other doors nearby the laboratory, or moving magnetic objects around the experimental setup. The simple difference between the first and the second half cycle with the time period of the half cycle, T , results in

$$D^+(T) - D^-(2T) = 2B_{12+13} - a_1T - 3a_2T^2 - 7a_3T^3. \quad (6)$$

Since this computation removes only the a_0 term, the remaining drift terms can add systematic effects to the extraction of B_{12+13} . To this end, we used a more effective computation on the data which applies a $[+1 \ -3 \ +3 \ -1]$ weighting to the mean value from each half cycle within two cycles [22, 43]:

$$D^+(T) - 3D^-(2T) + 3D^+(3T) - D^-(4T) = 8B_{12+13} - 6a_3T^3. \quad (7)$$

This weighting computation effectively eliminates the dominant slow drift terms up to second order. The remaining third- or higher-order drifts might become major systematic effects if the data is averaged for a long time and the statistical uncertainty is reduced. According to Eq. 7, the effective field magnitude B_{12+13} can be obtained by dividing the resulting value by a factor of 8 assuming that the remaining third order drift is negligible.

A histogram of the effective field magnitude B_{12+13} , extracted with the weighting computation from the magnetometer signals collected for 77 hours, is shown in Fig. 4. A fit with a Gaussian distribution to the histogram gives $B_{12+13} = (0.94 \pm 2.15) \times 10^{-16}$ T. According to Eq. 2, this equates to $\Delta E = (1.71 \pm 3.90) \times 10^{-20}$ eV with $\gamma = 2\pi \times 7.0 \times 10^9$ Hz/T [40]. The modulation method together with the weighting computation suppresses the major systematic effects below the statistical sensitivity of 2.15×10^{-16} T.

To experimentally constrain the interaction V_{12+13} from our SERF magnetometer-based experiment, we performed a Monte Carlo integration for the interaction potential P_{12+13} , as described above. Based on Eqs. 1 and 2, the experimental limit to the coupling strength f_{12+13} was estimated from dividing the experimental sensitivity of ΔE of 3.90×10^{-20} eV by

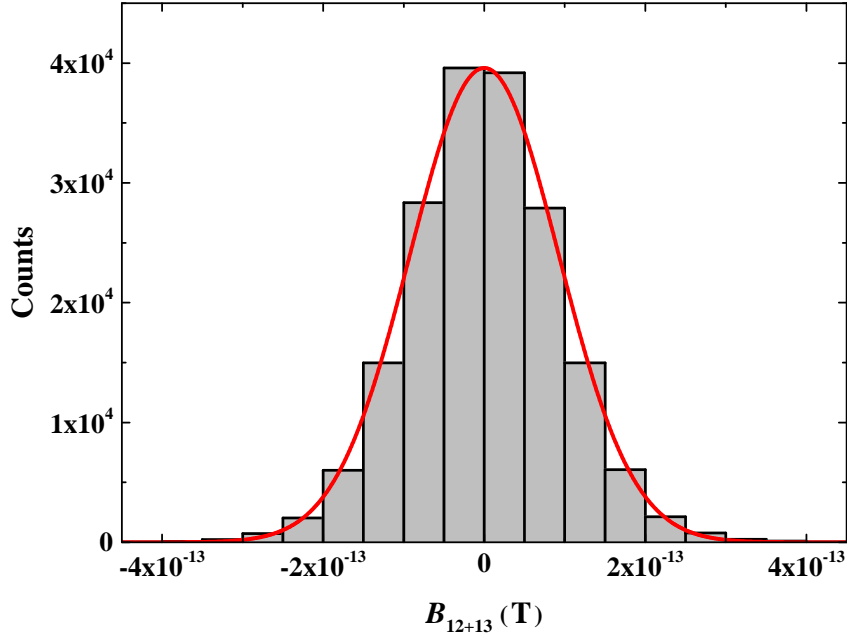


FIG. 4. Distribution of the magnitude of the effective field, B_{12+13} , obtained with the weighting computation from data collected for 77 h. The overlaid solid curve represents a fit with a Gaussian distribution to the data, which gives $B_{12+13} = (0.94 \pm 2.15) \times 10^{-16}$ T.

the interaction potential calculated at different interaction ranges [22]. Figure 5 shows the experimental limit to f_{12+13} in interaction ranges above 10^{-4} m (bottom axis), corresponding to the vector boson mass below 10^{-3} eV (top axis) with the data collection time of 77 hours.

DISCUSSION

Our experiment sets a new experimental limit on the parity-odd spin- and velocity-dependent interaction V_{12+13} for electrons in the vector boson mass ranges below 10^{-3} eV, which is essential for developing new directions in WISPs searches. One great advantage in our experiment is that the vector boson mass range can be simultaneously scanned, unlike the resonant cavity-based WISP-searching experiments, such as ADMX, which require tuning experimental parameters for each axion mass under investigation. Using this experimental method, recently, we also set a new experimental limit on the parity-even spin- and velocity-dependent interaction V_{4+5} between polarized electrons and unpolarized nucleons in the

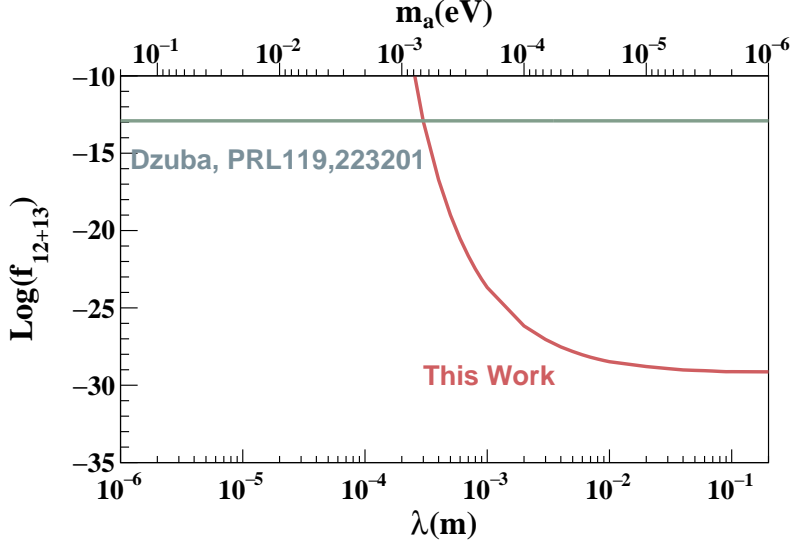


FIG. 5. Experimental constraint on the interaction V_{12+13} . The red curve indicates the experimental limit of our experiment on the exotic spin- and velocity-dependent interaction V_{12+13} between polarized Rb electrons inside the magnetometer’s vapor cell and unpolarized nucleons of the BGO mass as a function of the interaction range in the bottom axis and the vector boson mass in the top axis. This was derived with the experimental sensitivity of 2.15×10^{-16} T from data collected for 77 hours. Our SERF magnetometer-based experiment is sensitive for $m_a < 10^{-3}$ eV and $\lambda > 10^{-4}$ m. The gray line indicates the same coupling which can be also derived from PNC experiments [28] where the coupling has been scaled according to $f_{12+13} = 4g_A^e g_V^N$ [31]. Our experiment significantly enhances the constraint for f_{12+13} by 17 orders of magnitude beyond the PNC experiments.

sub-meV range of the vector boson mass [22]. These experimental results demonstrate the feasibility of our experimental approach using the SERF atomic magnetometer. Our experiments will play an important role in exploring the uninvestigated spin-dependent interactions for polarized electrons [23].

Further enhancement in the experimental sensitivity could be achievable. The SERF atomic magnetometer used in this work operates in a single-beam configuration in which a single circularly polarized laser beam is used to pump and probe the Rb electron spins [42]. The single-beam configuration is suboptimal in terms of magnetic field sensitivity. For an improved design, the magnetometer would use an orthogonal-beam configuration in which

the probe beam is perpendicular to the pump beam, and the laser beams' wavelengths are individually optimized. This modification can improve the sensitivity to $1 \text{ fT/Hz}^{1/2}$ immediately. Further work will bring the magnetometer close to the fundamental photon shot noise limit of subfemto-Tesla to atto-Tesla [44] by reducing the noise sources from laser frequency and intensity fluctuations, and the hybrid optical pumping [44].

In conclusion, we explored the exotic parity-odd spin- and velocity-dependent interaction V_{12+13} for polarized electrons based on an experimental approach utilizing a SERF atomic magnetometer. Our experiment sets a new experimental limit on the interaction in the interaction range higher than 10^{-4} m corresponding to the vector boson mass lower than 10^{-3} eV.

METHODS

Monte Carlo integration. The algorithm of the Monte Carlo integral is following:

- (1) 2^{20} random pairs of points inside both the volumes of the BGO mass and the Rb vapor cell are generated;
- (2) An interaction range λ between 10^{-1} to 10^{-6} m is assumed to calculate the interaction potential P_{12+13}^i between a randomly generated pair of points i ,

$$P_{12+13}^i = \frac{\hbar}{8\pi} (\hat{\sigma}_i \cdot \vec{v}) \frac{e^{-r_i/\lambda}}{r_i};$$

- (3) All the contributions to the potential are summed and normalized to give the average interaction potential for the nucleon density of BGO mass N_{BGO} :

$$P_{12+13} = N_{\text{BGO}} \frac{1}{2^{20}} \sum_i^{2^{20}} P_{12+13}^i; \quad (8)$$

- (4) The experimental limit to the coupling strength f_{12+13} is derived by dividing the experimental sensitivity of the energy shift ΔE for Rb atoms by the calculated average interaction potential;
- (5) The steps from (1) to (4) are repeated with another given interaction range between 10^{-1} to 10^{-6} m.

The Monte Carlo error can be ignored because the error numerically decreases as $1/\sqrt{N}$ where N is the number of random points, thus it is less than 1% with the 2^{20} random points.

SERF atomic magnetometer A SERF atomic magnetometer employed for the experiments, manufactured by QuSpin Inc., is a compact, self-contained unit with all the necessary optical components and can be readily operated using a control software. Practically, the SERF regime is achieved by operating in a near-zero magnetic field and by heating the Rb vapor; a SERF magnetometer is sensitive at low frequency below 100 Hz. It is mainly composed of a 3 mm cube ^{87}Rb vapor cell, a single semiconductor 795 nm laser for both optical pumping and probing, and silicon photodiodes [42]. The dimensions of the magnetometer module are: length 8 cm, width 1.4 cm, and height 2.1 cm. The cell temperature is around 160° for sufficiently large Rb density. The action of the laser beam creates a large number of polarized Rb electron spins in the vapor cell and its intensity transmitted through the cell is detected using the photodiode. The output from the photodiode is an analogue voltage signal and it can be converted to a magnetic field signal by applying a known calibration field to the vapor cell. In order to reduce the effects of the laser noise due to intensity fluctuation, the magnetometer uses a modulating field at 926 Hz [42]. The measured field at a certain low frequency is restored using a built-in lock-in amplifier and a low-pass filter.

DATA AVAILABILITY

The data that support the findings of this study are available from the corresponding author upon reasonable request.

ACKNOWLEDGEMENTS

The authors gratefully acknowledge this work was supported by the Los Alamos National Laboratory LDRD office through grant 20180129ER.

AUTHOR CONTRIBUTIONS

Y. J. K. designed and carried out the experiments, and analyzed the data. P.-H. C. performed the Monte-Carlo simulation and estimated the sensitivity. I. S. provided expertise in atomic magnetometers. S. N. and Y. J. K. built the experimental setup. All authors contributed to the manuscript.

COMPETING INTERESTS

The authors declare no competing financial interests.

- [1] J. E. Moody and F. Wilczek, *Phys. Rev. D* **30**, 130 (1984).
- [2] B. A. Dobrescu and I. Mocioiu, *J. High Energy Phys.* **2006**, 005 (2006).
- [3] P. Fadeev, Y. V. Stadnik, F. Ficek, M. G. Kozlov, V. V. Flambaum, and D. Budker, (2018), arXiv:1810.10364 [hep-ph].
- [4] J. Jaeckel and A. Ringwald, *Annu. Rev. Nucl. Part. Sci.* **60**, 405 (2010).
- [5] R. D. Peccei and H. R. Quinn, *Phys. Rev. Lett.* **38**, 1440 (1977).
- [6] S. Weinberg, *Phys. Rev. Lett.* **40**, 223 (1978).
- [7] F. Wilczek, *Phys. Rev. Lett.* **40**, 279 (1978).
- [8] P. Sikivie, “Axion cosmology,” in *Axions: Theory, Cosmology, and Experimental Searches*, edited by M. Kuster, G. Raffelt, and B. Beltrán (Springer Berlin Heidelberg, Berlin, Heidelberg, 2008) pp. 19–50.
- [9] L. D. Duffy and K. van Bibber, *New Journal of Physics* **11**, 105008 (2009).
- [10] B. Holdom, *Physics Letters B* **166**, 196 (1986).
- [11] T. Appelquist, B. A. Dobrescu, and A. R. Hopper, *Phys. Rev. D* **68**, 035012 (2003).
- [12] P. Langacker, *Rev. Mod. Phys.* **81**, 1199 (2009).
- [13] P. Arias, D. Cadamuro, M. Goodsell, J. Jaeckel, J. Redondo, and A. Ringwald, *JCAP* **1206**, 013 (2012), arXiv:1201.5902 [hep-ph].
- [14] R. Essig *et al.*, in *Proceedings, 2013 Community Summer Study on the Future of U.S. Particle Physics: Snowmass on the Mississippi (CSS2013): Minneapolis, MN, USA, July 29-August 6, 2013* (2013) arXiv:1311.0029 [hep-ph].
- [15] S. J. Asztalos, G. Carosi, C. Hagmann, D. Kinion, K. van Bibber, M. Hotz, L. J. Rosenberg, G. Rybka, J. Hoskins, J. Hwang, P. Sikivie, D. B. Tanner, R. Bradley, and J. Clarke, *Phys. Rev. Lett.* **104**, 041301 (2010).
- [16] C. Patrignani *et al.* (Particle Data Group), *Chin. Phys.* **C40**, 100001 (2016).
- [17] M. S. Safronova, D. Budker, D. DeMille, D. F. J. Kimball, A. Derevianko, and C. W. Clark, *Rev. Mod. Phys.* **90**, 025008 (2018).

- [18] G. D. Hammond, C. C. Speake, C. Trenkel, and A. P. Patón, *Phys. Rev. Lett.* **98**, 081101 (2007).
- [19] S. A. Hoedl, F. Fleischer, E. G. Adelberger, and B. R. Heckel, *Phys. Rev. Lett.* **106**, 041801 (2011).
- [20] P.-H. Chu, A. Dennis, C. B. Fu, H. Gao, R. Khatiwada, G. Laskaris, K. Li, E. Smith, W. M. Snow, H. Yan, and W. Zheng, *Phys. Rev. D* **87**, 011105 (2013).
- [21] X. Rong, M. Wang, J. Geng, X. Qin, M. Guo, M. Jiao, Y. Xie, P. Wang, P. Huang, F. Shi, Y.-F. Cai, C. Zou, and J. Du, *Nature Communications* **9** (2018).
- [22] Y. J. Kim, P.-H. Chu, and I. Savukov, *Phys. Rev. Lett.* **121**, 091802 (2018).
- [23] P.-H. Chu, Y. J. Kim, and I. Savukov, *Phys. Rev. D* **94**, 036002 (2016).
- [24] W. Happer and H. Tang, *Phys. Rev. Lett.* **31**, 273 (1973).
- [25] J. C. Allred, R. N. Lyman, T. W. Kornack, and M. V. Romalis, *Phys. Rev. Lett.* **89**, 130801 (2002).
- [26] T. D. Lee and C. N. Yang, *Phys. Rev.* **104**, 254 (1956).
- [27] C. S. Wu, E. Ambler, R. W. Hayward, D. D. Hoppes, and R. P. Hudson, *Phys. Rev.* **105**, 1413 (1957).
- [28] V. A. Dzuba, V. V. Flambaum, and Y. V. Stadnik, *Phys. Rev. Lett.* **119**, 223201 (2017).
- [29] E. M. Purcell and N. F. Ramsey, *Phys. Rev.* **78**, 807 (1950).
- [30] T. Chupp, P. Fierlinger, M. Ramsey-Musolf, and J. Singh, (2017), arXiv:1710.02504 [physics.atom-ph].
- [31] T. M. Leslie, E. Weisman, R. Khatiwada, and J. C. Long, *Phys. Rev. D* **89**, 114022 (2014).
- [32] P. Fayet, *Nuclear Physics B* **347**, 743 (1990).
- [33] H. Yan and W. M. Snow, *Phys. Rev. Lett.* **110**, 082003 (2013).
- [34] E. G. Adelberger and T. A. Wagner, *Phys. Rev. D* **88**, 031101 (2013).
- [35] H. Yan, G. A. Sun, S. M. Peng, Y. Zhang, C. Fu, H. Guo, and B. Q. Liu, *Phys. Rev. Lett.* **115**, 182001 (2015).
- [36] B. R. Heckel, C. E. Cramer, T. S. Cook, E. G. Adelberger, S. Schlamminger, and U. Schmidt, *Phys. Rev. Lett.* **97**, 021603 (2006).
- [37] B. R. Heckel, E. G. Adelberger, C. E. Cramer, T. S. Cook, S. Schlamminger, and U. Schmidt, *Phys. Rev. D* **78**, 092006 (2008).

- [38] F. Ficek, D. F. J. Kimball, M. G. Kozlov, N. Leefer, S. Pustelny, and D. Budker, *Phys. Rev. A* **95**, 032505 (2017).
- [39] F. Ficek, P. Fadeev, V. V. Flambaum, D. F. Jackson Kimball, M. G. Kozlov, Y. V. Stadnik, and D. Budker, *Phys. Rev. Lett.* **120**, 183002 (2018).
- [40] T. Karaulanov, I. Savukov, and Y. J. Kim, *Meas. Sci. Technol.* **27**, 055002 (2016).
- [41] QuSpin Inc. Available at: <http://www.quspin.com/>.
- [42] I. Savukov, Y. J. Kim, V. Shah, and M. G. Boshier, *Meas. Sci. Technol.* **28**, 035104 (2017).
- [43] Y. J. Kim, C.-Y. Liu, S. K. Lamoreaux, G. Visser, B. Kunkler, A. N. Matlashov, J. C. Long, and T. G. Reddy, *Phys. Rev. D* **91**, 102004 (2015).
- [44] J.-H. Liu, D.-Y. Jing, L.-L. Wang, Y. Li, W. Quan, J.-C. Fang, and W.-M. Liu, *Scientific Reports* **7**, 6776 (2017).